Available online at www.sciencedirect.com
ScienceDirect
International Journal of Heat and Mass Transfer 51 (2008) 1646–1657
International Journal of HEAT and MASS TRANSFER
www.elsevier.com/locate/ijhmt

Numerical simulation of film boiling on a sphere with a volume of fluid interface tracking method

M.H. Yuan *, Y.H. Yang, T.S. Li, Z.H. Hu

School of Nuclear Science and Engineering, Shanghai Jiao Tong University, Shanghai 200240, China

Received 23 March 2007; received in revised form 18 June 2007
Available online 21 September 2007

Abstract

This paper presents a numerical method for the simulation of boiling flows on non-orthogonal body-fitted coordinates. The volume-of-fluid (VOF) method based on piecewise linear interface construction (PLIC) is used to track liquid–vapor interface and is extended to body-fitted coordinates. Some special treatment is taken to deal with the discontinuous velocity field due to phase change at the interface. A double staggered grid with the SIMPLE method is adopted to solve the flow field. This method is used to simulate natural convection film boiling and forced convection film boiling on a sphere at saturated conditions. The simulation results are compared with analytical correlations and experimental data.

Keywords: VOF; Phase change; Film boiling

1. Introduction

Film boiling is a major heat transfer mechanism that occurs when wall temperature is much higher than the saturation temperature of the liquid. It is widely used in cryogenic systems, metallurgic industries and other areas where extremely high temperature differences are involved. Film boiling is also a major concern in the nuclear reactor safety analyses. In the field of severe accident research for light water reactors (LWRs), steam explosion caused by the contact of molten core and coolant is recognized as one of the potential threats to the integrity of the containment or the reactor pressure vessel [1]. It is widely understood that a steam explosion proceeds in four phenomenological stages: premixing, triggering, propagation and expansion. During the premixing stage hot liquid in the form of particles is mixed with the pool of liquid coolant. There is relative movement between the particles and coolant, but the particles are prevented from intimate contact with coolant by a vapor blanket. If this vapor film is stable, a substantial volume of this coarse mixture might be produced. Knowledge of the events in this mixing stage, leading to vapor collapse, is particularly important. Various models and experiments of film boiling heat transfer from a sphere have been published [2–10].

With the advent of numerical techniques for the simulation of interfacial flows with liquid–vapor phase change in the past few years, the prospect of using numerical simulations to study the transient and dynamic aspects of boiling flows has become very promising. Welch [11] simulated a fully deformable, two-dimensional bubble using moving mesh and the interface is tracked by nodes representing the liquid and vapor sides at the same spatial location. Son and Dhir [12] used a coordinate transformation technique supplemented by a numerical grid generation method to simulate film boiling for both two-dimensional and axisymmetric flows. Many other numerical studies of film boiling are available in the open literature, such as that of Juric and Tryggvason [13] developing a front-tracking method, Son and Dhir [14] using a level set method and Welch and Wilson [15] using a volume-of-fluid (VOF) method.

* Corresponding author. Tel.: +86 21 34205301; fax: +86 21 34205182.
E-mail address: mhyuan@sjtu.edu.cn (M.H. Yuan).

0017-9310/$ - see front matter © 2007 Elsevier Ltd. All rights reserved.
doi:10.1016/j.ijheatmasstransfer.2007.07.037

Nomenclature

C	fractional volume function
C_p	specific heat
d	distance
D	diameter
g	gravitational acceleration
h_{lg}	latent heat
h	heat transfer coefficient
J	Jacobian of transformation
K	conductivity
m	mass flux
n	unit normal vector
Nu	Nussselt number, hD/k_g
p	pressure
p_∞	system pressure
q	heat flux
S	interface
t	time
Δt	time step
T	temperature
ΔT	temperature difference
u	velocity in the x-direction
V	velocity in the y-direction
U	contravariant velocity component
V	contravariant velocity component, a volume
V_∞	inlet velocity
x	Cartesian coordinates component
y	Cartesian coordinates component

Greek symbols

α	geometry coefficient
β	geometry coefficient
γ	geometry coefficient
Γ	volume expansion or contraction
δ	Dirac distribution
ε	radiation emissivity
ζ	general curvilinear coordinates
η	general curvilinear coordinates
θ	angle
κ	curvature
μ	dynamic viscosity
ν	kinematical viscosity
ρ	density
σ	surface tension
σ_b	Stefan–Boltzmann constant
Φ	source term for latent heat
χ	characteristic function
Ψ	radiant heat in phase change

Subscripts

c	convection
g	vapor phase
l	liquid phase
sat	saturation
r	radiation
t	total heat flux
w	wall

In this paper, a numerical method for the simulation of boiling flows on non-orthogonal body-fitted coordinates is presented. The volume-of-fluid (VOF) method is used to track the interface and some special treatment is taken to deal with the discontinuous velocity field due to the rapid mass transfer at the liquid–vapor interface. The VOF method [16–19] is a popular interface tracking algorithm that has proven to be a useful and robust tool since its development over two decades ago. It has therefore become a frequent choice in Eulerian models of interfacial flows, especially those flows where interfaces undergo topology changes. A double staggered grid with the SIMPLE method [20] is adopted to solve the flow field because the discontinuous velocity field and the discontinuous body force (gravity) field at the sharp interface make a collocated grid which is more popular for body-fitted coordinates inapplicable. The method is used to simulate natural convection film boiling and forced convection film boiling on a sphere at saturated conditions, and the simulation results are compared with analytical correlations and experimental data.

2. Physical modeling

The liquid and vapor are all considered as incompressible Newtonian fluids, so the momentum equation in body-fitted coordinates can be expressed as

$$\begin{aligned}&\frac{\partial}{\partial t}(\rho u)+\frac{1}{J}\frac{\partial}{\partial \xi}(\rho U u)+\frac{1}{J}\frac{\partial}{\partial \eta}(\rho V u)\\&=-\frac{1}{J}(p_\xi y_\eta - p_\eta y_\xi)+\rho g_x\\&\quad+\frac{1}{J}\frac{\partial}{\partial \xi}\left[\frac{\mu}{J}(\alpha u_\xi-\beta u_\eta)\right]+\frac{1}{J}\frac{\partial}{\partial \eta}\left[\frac{\mu}{J}(-\beta u_\xi+\gamma u_\eta)\right]+2\sigma\kappa\delta_s n_x,\end{aligned} \tag{1}$$

$$\begin{aligned}&\frac{\partial}{\partial t}(\rho v)+\frac{1}{J}\frac{\partial}{\partial \xi}(\rho U v)+\frac{1}{J}\frac{\partial}{\partial \eta}(\rho V v)\\&=-\frac{1}{J}(-p_\xi x_\eta + p_\eta x_\xi)+\rho g_y\\&\quad+\frac{1}{J}\frac{\partial}{\partial \xi}\left[\frac{\mu}{J}(\alpha v_\xi-\beta v_\eta)\right]+\frac{1}{J}\frac{\partial}{\partial \eta}\left[\frac{\mu}{J}(-\beta v_\xi+\gamma v_\eta)\right]+2\sigma\kappa\delta_s n_y.\end{aligned} \tag{2}$$

Surface tension in the above equations is treated with Continuum Surface Force (CSF) model proposed in [21]. Contravariant velocity components U, V, Jacobian of the transformation J and geometry coefficients dependent on the coordinate transformation α, β, γ are defined as below:

$$U = uy_\eta - vx_\eta, V = vx_\xi - uy_\xi, \tag{3}$$

$$J = x_\xi y_\eta - x_\eta y_\xi, \alpha = x_\eta^2 + y_\eta^2, \beta = x_\xi x_\eta + y_\xi y_\eta, \gamma = x_\xi^2 + y_\xi^2. \tag{4}$$

The energy equation is as below:

$$\frac{\partial}{\partial t}(\rho T) + \frac{1}{J}\frac{\partial}{\partial \xi}(\rho C_p U T) + \frac{1}{J}\frac{\partial}{\partial \eta}(\rho C_p V T) = \frac{1}{J}\frac{\partial}{\partial \xi}\left[\frac{k}{J}(\alpha T_\xi - \beta T_\eta)\right] + \frac{1}{J}\frac{\partial}{\partial \eta}\left[\frac{k}{J}(-\beta T_\xi + \gamma T_\eta)\right] + \Phi. \tag{5}$$

Φ is a source for the latent heat due to phase change at the interface. The continuity equation is as follows:

$$\frac{1}{J}\frac{\partial}{\partial \xi}U + \frac{1}{J}\frac{\partial}{\partial \eta}V = \Gamma, \tag{6}$$

where Γ is the volume expansion or contraction due to the mass exchange between two fluids with different densities at their interface. The material properties in the above equation are constant in each phase but may vary from phase to phase. These equations may be viewed as a "one-fluid formulation" as they are expressed at any position.

In order to distinguish whether a point in the domain is occupied by liquid or vapor, a characteristic function χ with value 1 in one phase and 0 in another phase is introduced [16], then

$$\frac{\partial}{\partial t}\chi + \frac{1}{J}\frac{\partial}{\partial \xi}(U\chi) + \frac{1}{J}\frac{\partial}{\partial \eta}(V\chi) = 0. \tag{7}$$

The fractional volume function C in the VOF method may be viewed as a discretization of the characteristic function χ, although the application of standard algorithms for hyperbolic equations to Eq. (7) does not always give the best results.

When evaporation or condensation occurs at the interface, Γ is related to the interfacial mass flux m by

$$\int\int\int_V \Gamma \, dv = \int\int_S m\left(\frac{1}{\rho_g} - \frac{1}{\rho_l}\right) ds, \tag{8}$$

where V is a domain, S is the interface in V, as shown in Fig. 1. In derivation of Eq. (8), the incompressibility of both phases is used.

Energy transfer at the interface during phase change with radiation heat transfer can be written as

$$(\vec{q}_l - \vec{q}_g)\cdot\vec{n} + \Psi = \left(k_l\frac{\partial T}{\partial n}\bigg|_l - k_g\frac{\partial T}{\partial n}\bigg|_g\right) + \Psi = mh_{lg}. \tag{9}$$

Here $\boldsymbol{q}_l$ and $\boldsymbol{q}_g$ are heat flux vectors in liquid side and vapor side of the interface, $\boldsymbol{n}$ is the unit normal vector to the interface and Ψ is the radiation energy participating in phase change. To derive Eq. (9), kinetic energy and viscous work are neglected. The interface temperature T_s is assumed to be equal to the equilibrium saturation temperature corresponding to the system pressure:

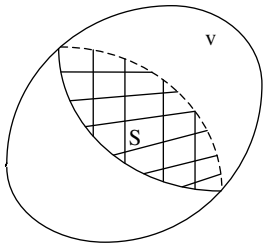

Fig. 1. A domain V includes an interface S.

$$T_s = T_{sat}(P_\infty). \tag{10}$$

If the temperature of the hot wall is high, radiation heat transfer cannot be neglected. Because the vapor film is always very thin, the vapor is regarded as non-participating media for radiation, and all the radiant energy is assumed to be absorbed at the interface and acts as an energy source for evaporation. The radiant heat flux q_r at the hot wall is expressed as

$$q_r = \varepsilon\sigma_b T_w^4. \tag{11}$$

Based on the location and orientation of the liquid–vapor interface, the radiant heat from a hot wall is distributed to the distant interface approximately. Then Ψ in Eq. (9) is obtained accordingly. The calculation of Ψ is strongly dependent on a specific case. For instance, radiant energy absorbed at the vapor–liquid interface surrounding a hot sphere with radius r can be expressed as

$$\Psi = q_r\left(\frac{r}{d}\right)^2\cos\theta, \tag{12}$$

where d is the distance from the sphere center to the local interface, θ is the angle between the normal vector to the interface and the vector from sphere center to the local interface.

3. Numerical method

Eqs. (1), (2), (5) and (6) are discretized with a finite volume method in non-orthogonal body-fitted coordinates. Pressure-velocity linkage is resolved with the SIMPLE algorithm, in which Eq. (6) is used to construct an equation for pressure correction. In space discretization, the second-order central differencing scheme is used for diffusion terms and the MUSCL scheme is used for convection terms. A first order backward implicit approach is employed for the time derivative.

3.1. Double staggered grid

In the solution of Navier–Stokes equations by finite volume methods, it is assumed that the discretized velocities

that are used to satisfy the continuity equation (6) (from which the pressure distribution is determined) should also simultaneously satisfy the momentum equations (1), and 2). In the computation of flows in complex geometries using non-orthogonal body-fitted grids, several practical advantages are achieved by employing a collocated grid arrangement in which the velocities and pressures are stored at the same location, that is, at the grid node [22]. The collocated arrangement was out of favor for a long time for incompressible flow computation due to the difficulties in the pressure-velocity coupling and occurrence of oscillations in the pressure. The cure for this problem was first proposed by Rhie and Chow [23], in which the cell face velocities are interpolated via the momentum-interpolation. Although the Rhie and Chow's procedure has enjoyed considerable popularity, it predicts spurious cell face velocities when local variation of pressure departs considerably from linearity [24].

In the VOF method, a sharp interface is maintained through the computation, so if the density ratio of the two fluids is large and gravity force is included, the pressure variation near the interface is far away from linearity. A one-dimensional problem is used to illustrate this situation, as shown in Fig. 2. The vapor is above the liquid and the liquid–vapor interface is contained in the cell of node P. Both vapor and liquid are kept static with a downward gravity force. The pressure distribution is shown in Fig. 2b. It is obvious that near the sharp interface, the gradient of pressure changes abruptly if liquid–vapor density ratio is large. It should be noted that this nonlinear local variation of pressure filed can not be diminished by grid refinement because the sharp interface is always maintained with the VOF method.

In a collocated grid arrangement, the velocities are stored at the grid nodes and the cell face velocities used in the continuity equation are calculated by interpolating the velocities at two nodes on either side of the face. If phase change occurs, the velocity field is discontinuous at the liquid–vapor interface, so large errors could be introduced during the interpolation. As shown in Fig. 3, evaporation occurs at the liquid–vapor interface contained in the

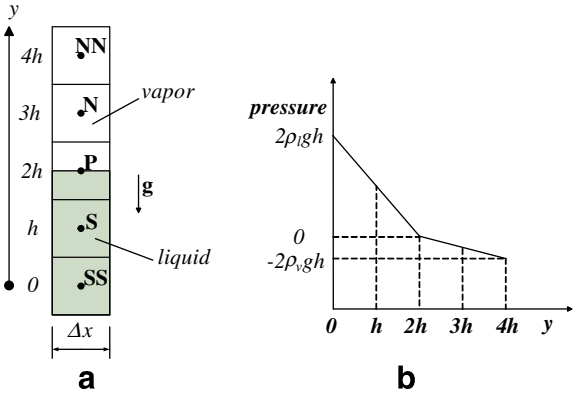

Fig. 2. Pressure variation at the interface in a one-dimensional problem.

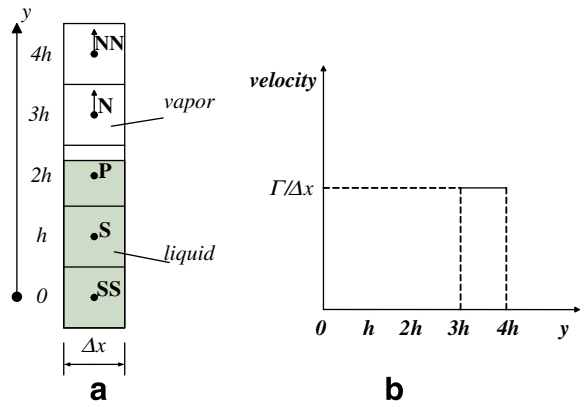

Fig. 3. Discontinuous velocity at the interface with evaporation in a one-dimensional problem.

cell of node P and the volume expansion due to evaporation is Γ. The liquid is kept static, so the vapor velocities at node N and node NN equal $\Gamma/\Delta x$. It is obvious that the velocity at north cell face of node P is also $\Gamma/\Delta x$ in this case. But if it is calculated by interpolating of the velocities at node P and node N, a wrong value of $\Gamma/2\Delta x$ will be obtained.

Because of the above difficulties, the collocated grid arrangement is not suitable for the calculation of interfacial flows with a large density ratio and phase change, so a staggered grid seems to be a good choice. But as pointed out in [22], in body-fitted coordinates, the grid lines often change their direction significantly, and the velocity component stored at the cell face may make no contribution to the mass flux through that face, as it is parallel to the face as shown in Fig. 4. This problem can be overcome if all Cartesian velocity components are stored at each cell face. With such a variable arrangement, two staggered grids have to be used, which are named as double staggered grid in two-dimensions [25]. The first grid is a MAC mesh with pressure arranged at the cell center and velocity components at the cell faces. The second grid is so displaced that its corners correspond to the center of the first grid. In the second grid the pressure is placed at the corner of the first grid, as shown in Fig. 4. With these two grids, although the velocity components u and v make no contribution to mass flux for the cell P belonging to the first grid (solid line),

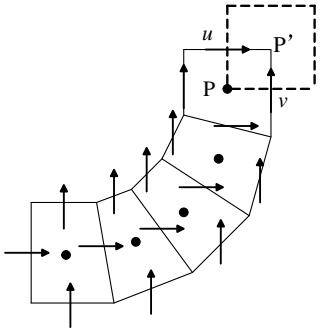

Fig. 4. Staggered arrangement on a non-orthogonal grid.

they contribute to the mass flux for the cell P' belonging to the second grid (dashed line). So the proper coupling of velocities and pressure is ensured and oscillations are avoided. Although this double staggered grid has no advantages over collocated grid for normal flow calculations, it is a very appropriate choice for the calculation of interfacial flows with a large density ratio and phase change. More details of the double staggered grid can be seen in [25].

3.2. VOF/PLIC on body-fitted coordinates

Eq. (7) is solved with the VOF method, in which a fractional volume function C indicates the fraction of a mesh cell that is filled with fluid of a particular type, e.g. the liquid phase. So $C = 1$ indicates a liquid cell, $C = 0$ a vapor cell and $0 < 1 < C$ a mixture cell. Material properties in Eqs. (1), (2) and (5) are determined as below:

$$\begin{aligned} \rho &= \rho_l C + \rho_g (1 - C), \\ \mu &= \mu_l C + \mu_g (1 - C), \\ k &= k_l C + k_g (1 - C). \end{aligned} \tag{13}$$

In order to get the C field at a new time point, the flux of the volume of a particular fluid through a cell face during the corresponding time step has to been obtained. An important characteristic of the VOF method is that the flux is calculated based on the geometric information of the liquid–vapor interface which may cut through a single cell. The geometric information of the interface is obtained through reconstruction. The orientation and location of the interface is reconstructed by the known C field at the old time. There are several different VOF algorithms with different reconstruction schemes, such as SOLA-VOF [16], FLAIR method [18], Youngs VOF [19] etc. Among those methods, Youngs VOF method is proved to perform well in most situations and is employed in our simulations. Youngs VOF uses a line segment (in two dimension) defined by a slope and intercept to represent the interface in a mixture cell, which is usually called PLIC (piecewise linear interface construction). Then the flux of volume of a particular fluid through a mixture cell face during a time step could be computed and the C field at the new time is updated.

Although in physical domain grid cells are irregular quadrilaterals with body-fitted coordinates, in the computation domain after coordinates transformation grid cells are all uniform rectangles, as shown in Fig. 5. So the VOF/PLIC could be applied to solve Eq. (7) with few modifications. For example, flux of volume of liquid through the right face of a mixture cell is indicated in Fig. 6 with the shaded area.

Two test problems from [26] are used to verify the VOF/PLIC method in body-fitted coordinates. In the tests, analytic velocity fields are chosen and no attempt is made to couple the advection of C to the solution of the momentum equations. A parallelogram domain and a 200×200 mesh

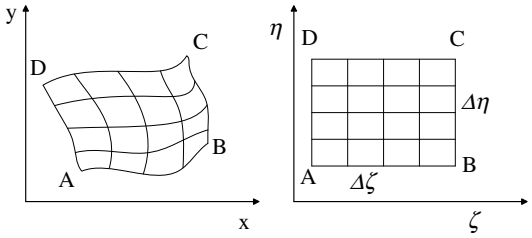

Fig. 5. A physical domain and the computational domain after coordinate transformation.

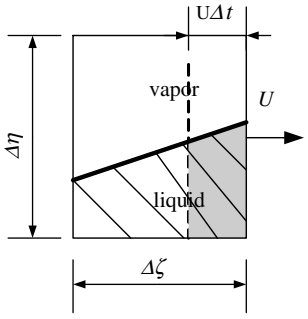

Fig. 6. In a mixture cell, a line segment represents an interface. The flux of volume of liquid through right face of the cell is indicated with shaded area. U is the contravariant velocity component at the right face of this cell, and Δt is the time step during which the volume is transported.

are chosen. The first test problem is to advect a hollow square in a unidirectional velocity field $(u, v) = (2, 1)$ for approximately 500 time steps (with a Courant number of 0.25). The result is shown in Fig. 7, in which contour levels of $C = 0.025$, 0.5 and 0.975 are displayed.

In the second test problem, a shearing flow field is chosen:

$$u(x, y) = \cos x \sin y, v(x, y) = -\sin x, \cos y. \tag{14}$$

The simulation is integrated forward in time for 1000 steps (with a Courant number of 0.25) before reversing the sign of the velocity field and integrating for an additional 1000 steps. A perfect advection scheme would return the initial C configuration. The initial condition is a circle. The shapes after forward and reverse integration are shown in Fig. 8.

Comparing the present numerical results to those given in [26], the VOF/PLIC method is proved to perform successfully in non-orthogonal coordinates as in Cartesian coordinates.

3.3. Special strategy to deal with phase change at interface

The VOF/PLIC algorithm is applicable to various situations, but when phase change occurs at the interface, some problems in the calculation of the flux of fluid volume through a cell face appear. This is shown in Fig. 9, in which the mixture cell contains both vapor and liquid and evaporation exists at the interface. It is assumed that all the veloc-

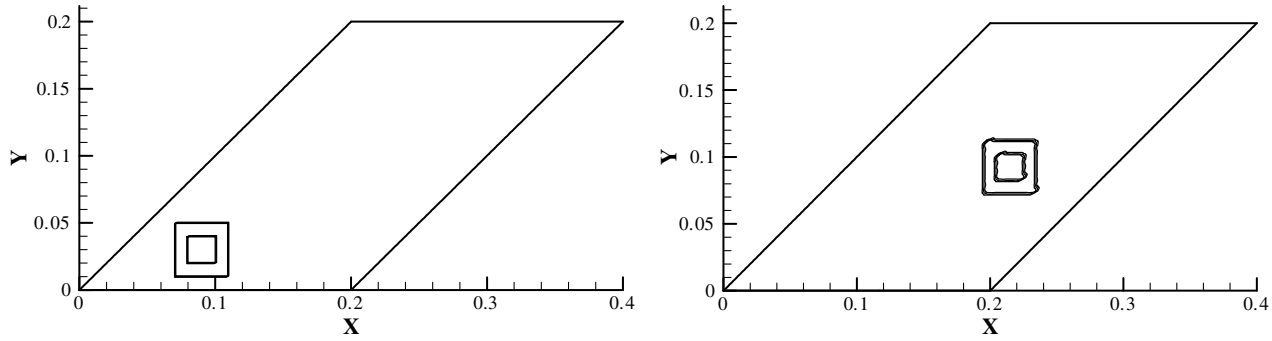

Fig. 7. Contour of C before and after advection in a unidirectional velocity field.

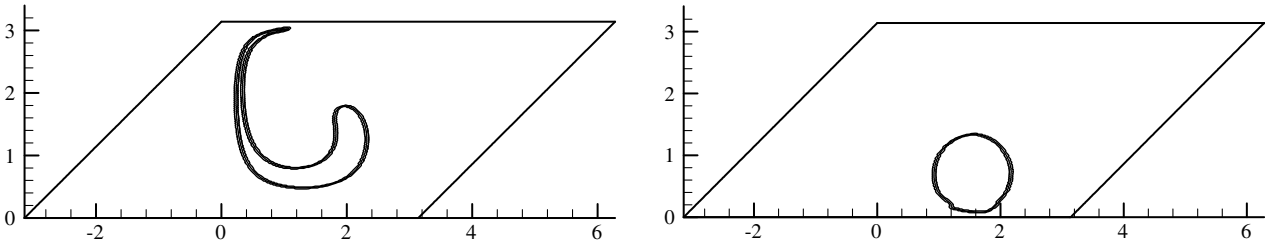

Fig. 8. Contour of C after forward and reverse integration in a shearing flow field.

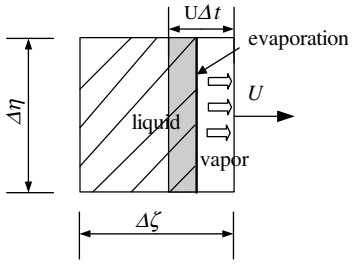

Fig. 9. In a mixture cell, evaporation occurs at the interface. The "false" flux of volume of liquid through the right surface of the cell with VOF/PLIC is indicated with shaded area. U is contravariant velocity component at the right face of this cell, and Δt is the time step during which the volume is transported.

ities are zero except the one located at the right face of the cell. Because vapor is generated continuously at the interface, the contravariant velocity at the right face is toward outside of the cell. With the VOF/PLIC method, which tracks the volume fraction of liquid for instance, the flux of volume of liquid through the right face of the cell is calculated by the shaded area, as shown in Fig. 9. It is obvious that this flux is not really transported, because in such situation, no liquid is transported through the right face of the cell, and all the fluid passing the right face is vapor.

Faced with such a problem, some special treatment has to be taken to find the real volume of fluid which is transported through a cell face in a mixture cell with phase change. However, the interface which is represented by a line segment could have arbitrary locations and orientations in a mixture cell and the velocity field is also unpredictable in advance, so it is rather difficult to identify which part of fluid volume is really transported. In this paper, an approximating strategy is used to overcome this problem. By this strategy, volume expansion or contraction due to mass exchange, i.e. Γ in Eq. (6), is moved from the mixture cell where phase change really occurs to the nearest vapor cell. So with this strategy, the velocity field is divergence free for all the mixture cells. Then the VOF/PLIC method is applicable to the mixture cells without any modifications to the algorithm except that the volume of liquid which has evaporated should be subtracted from the mixture cell. As for the vapor cell with volume expansion or contraction, no problem exits in the calculation of flux of liquid volume through cell face since liquid is the tracked phase and only the flux out of a cell is calculated. Then the flux of liquid volume out of a vapor cell is always zero. When Γ is moved from the mixture cell to the nearest vapor cell, an additional deviation from the exact solution is introduced. A fine grid could reduce this deviation. In the application of this strategy, because of the various interface shape, it is possible that some vapor cells get a much larger Γ than their neighbor cells. Therefore smoothing of Γ in the vapor cells within one or two grids could improve the performance of the algorithm.

3.4. Procedure of the whole algorithm

The procedure of the whole algorithm is summarized as follows:

1. Based on the previous C field and velocity field, the VOF/PLIC method is used to obtain the new C field.
2. Surface tension is calculated with the Continuum Surface Force (CSF) model.

3. With the new C field, material properties in Eqs. (1), (2) and (5) are obtained.
4. Energy equation (5) is solved, and new temperature is obtained.
5. The new C field is also used to determine the interface location and orientation. The radiation heat flux Ψ is calculated at the interface with phase change. Together with the new temperature field, Eq. (9) is used to calculate the interfacial mass flux m.
6. Eq. (8) is used to compute volume expansion or contraction, i.e. Γ in Eq. (6), and then Γ is moved from a mixture cell to the nearest vapor cell.
7. Eqs. (1), (2) and (6) are solved iteratively with the SIMPLE method to get the new velocity field.

The algorithm is second order in space and first order in time. The VOF/PLIC method has a time step limit. The explicit treatment of surface tension in CSF model has a stricter restriction to the time step [21]. So the first order differencing in time is accurate enough.

4. Simulation results and discussion

4.1. Natural convection film boiling on a sphere

An analytical solution for the natural convection film boiling on a sphere was first reported by Frederking and Clark [27], where the equations for the boundary layer in a vapor film, which was assumed to be smooth and surrounding the sphere, were solved by simplifying the equations and balancing integral momentum and energy. The correlation for Nusselt number is as below:

$$Nu = 0.586\left(Ra\frac{h_{fg}}{c_{pg}}\Delta T\right)^{1/4}, \quad Ra = \frac{gC_{pg}(\rho_l-\rho_g)D^3}{k_g v_g}. \tag{15}$$

Dhir and Lienhard [28] got a similar correlation:

$$Nu = 0.67\left[\frac{(\rho_l-\rho_g)gh'_{fg}D^3}{v_g k_g(T_w-T_{sat})}\right]^{1/4}, \quad h'_{fg} = h_{fg}\left(1+0.34\frac{c_{pg}\Delta T}{h_{fg}}\right). \tag{16}$$

Dhir and Purohit [6] did an experiment with spheres of steel, copper, and silver in water. They found that the properties of the sphere do not affect the heat transfer coefficient provided a stable film exists. When they correlated their data at saturated condition, they got:

$$Nu = 0.8\left[\frac{g(\rho_l-\rho_g)h_{fg}D^3}{v_g k_g(T_w-T_{sat})}\right]^{1/4}. \tag{17}$$

In addition to the above correlations, other authors have obtained different correlations analytically and experimentally which are reviewed by Liu and Theofanous [9].

In the simulations carried out in the present study, the liquid properties are $\rho_l = 958.0$ kg/m^3, $\mu_l = 0.000279$ kg/m s, $k_l = 0.680$ W/m k, $Cp_l = 4217$ J/kg K and the vapor properties are $\rho_g = 0.2579$ kg/m^3, $\mu_g = 0.0000297$ kg/m s, $k_g = 0.0637$ W/m k, $Cp_g = 2186$ J/kg K. Other parameters are set as surface tension $\sigma = 0.0589$ N/m, saturation temperature $T_s = 373$ K, latent heat $h_{lg} = 2257000$ J/kg, gravity $g = 9.8$ m/s^2. In this simulation, thermal radiation is not considered.

We take advantage of the symmetry in this problem and a computational domain of 0.1 m × 0.2 m is used. The sphere diameter is 0.00635 m and the temperature of the sphere surface is kept 1063 K. The grid and boundary conditions are shown in Fig. 10. Initially, the sphere is immersed in water and the distance from the sphere center to the water surface is 0.02 m. A vapor film of 0.7 mm thickness is initialized around the sphere.

At first, results of a convergence study are presented to ensure the adequacy of the grid resolution. Three grid resolutions 60 × 60, 120 × 120, and 180 × 180 are considered. A lot of grids are placed in the boundary layer near the sphere to capture the thin vapor film and the minimum spacing of the finest grid near the sphere is about 5×10^{-6} m. Fig. 11 shows the liquid–vapor interface movement on the three grids as the first bubble forms at the rear part of the sphere and leaves the vapor film. Fig. 12 shows the convective heat transfer coefficient h_c during the transient. From these figures, it is concluded that the grid resolution of 120 × 120 adequately represents the case under consideration.

There is always a periodic generation and detachment of vapor bubbles on the rear part of the sphere and the whole vapor surface is wavy as observed in experiment [9]. The convective heat transfer coefficient largely dependent on the vapor film thickness also changes periodically. Fig. 13 shows the Nu number during five periods of vapor bubble generation and detachment. The values of Nu number predicted by the correlations mentioned above are also displayed in Fig. 13. From this figure, it is seen that the Nu

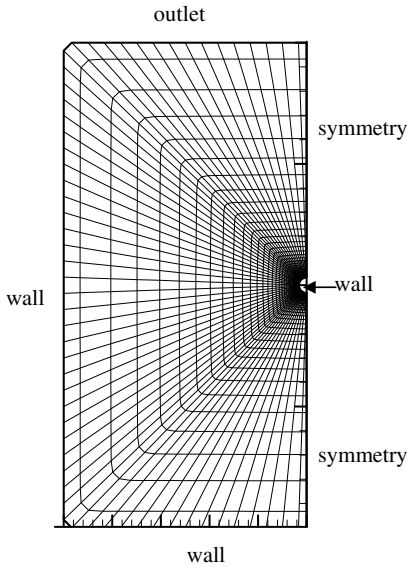

Fig. 10. Grid and boundary conditions for the simulation of natural convection film boiling on a sphere.

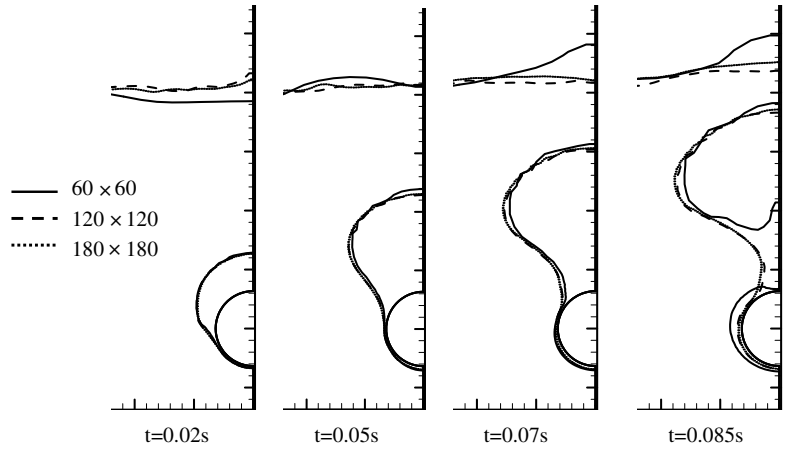

Fig. 11. Liquid–vapor interface movement as the first bubble forms at the rear part of the sphere and leaves the vapor film for three different grid resolutions.

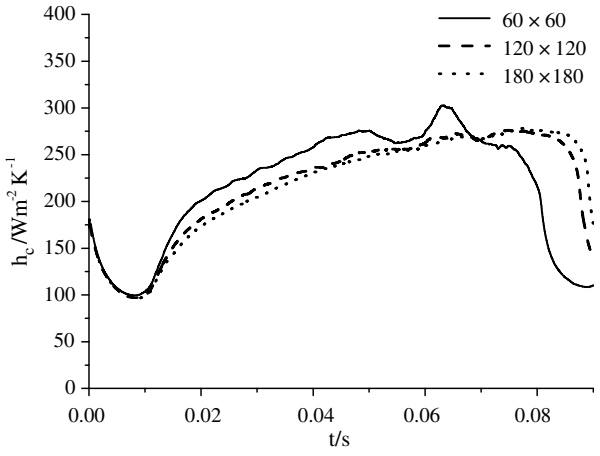

Fig. 12. Convective heat transfer coefficients for three different grid resolutions.

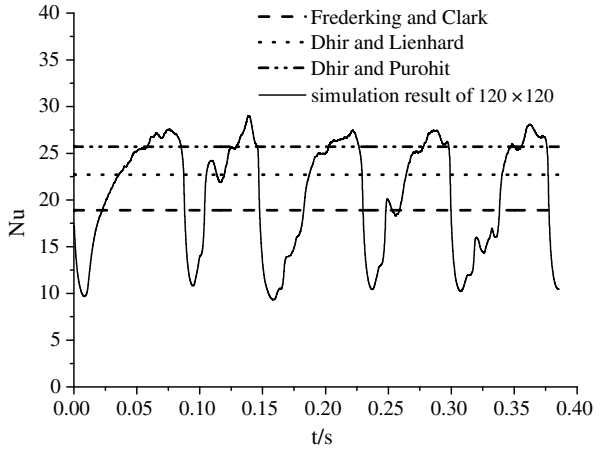

Fig. 13. *Nu* numbers during five periods of vapor bubble generation and detachment.

numbers predicted by Eqs. (15) and (16) are close to the averaged *Nu* number obtained with the simulation and Eq. (17) gives a higher value. It should be noted that Dhir and Purohit's experiment [6] is around the minimum film boiling temperature and may be partially in transition boiling regime, so Dhir and Purohit's correlation may overestimate film boiling heat transfer from a sphere.

4.2. Forced convection film boiling on a sphere

Film boiling from a moving sphere or a sphere submerged in flowing liquid differs from natural convection film boiling in the way that the vapor flow field is affected by the momentum exchange with the liquid flow at the liquid–vapor interface in addition to the buoyancy force.

Only a few experimental investigations of forced convection film boiling from spheres have been made. Stevens and Witte [7], Walford [8], Jacobson and Shair [29], Dhir and Purohit [6] have performed quenching tests using spheres of various sizes and materials, moving through various liquids. Most of these data are unsuitable for comparison to numerical simulation, because they lack some required details, such as instantaneous surface temperature and heat flux. The new experimental data base provided by Liu and Theofanous [9] consists of very high temperature film boiling (pure film boiling with the sphere temperature higher than the quenching point) in all the flow regimes and the film boiling heat transfer data can be obtained in their experiments. So their data are suitable for comparison to the present simulations.

Three cases from Liu and Theofanous's experiments [9] are chosen as in Table 1. In these cases, the sphere diameter is 6.35 mm and the water is kept saturated.

Table 1
Three experimental cases of forced convection film boiling on a sphere for numerical simulation

Case	V_∞ (m s^{-1})	*Fr*	T_w (K)	h_t (W m^{-2} K^{-1})	h_c (W m^{-2} K^{-1})
1	0.955	14.24	1061	369.57	314.95
2	0.538	4.515	1012	324.74	276.25
3	1.838	52.767	999	457.60	410.59

In these simulations, the liquid properties and vapor properties are same as those used in the natural convection film boiling simulation. Thermal radiation is included here, with Stefan–Boltzmann constant $\sigma_b = 5.67 \times 10^{-8}$, emissivity $\varepsilon = 0.7$. A grid resolution 120×120 is used. The computation domain and boundary conditions are similar to those of the natural convection, except the bottom boundary in Fig. 10 is changed from wall to an inlet boundary.

In the first case, the sphere temperature is set as 1061 K and the inlet velocity 0.955 m/s. Initially the sphere is above the water and the sphere center is 0.01 m away from the water surface. The movement of the liquid–vapor interface in the simulation is shown in Fig. 14. The vapor film at the front part of the sphere is thin and wavy. A large and long vapor wake can be seen. Vapor slugs detach from the trail of the vapor wake when the wake becomes too long. At $t = 0.0644$ s, the velocity field in the vapor film at the front part of the sphere is shown in Fig. 15. The parabolic distribution of velocity along the radial direction in the vapor film is in accordance with the analytical models [2–6]. A new experimental picture of a ZrO_2 sphere of diameter 6.35 mm at 1200 K falling to saturated water is shown in Fig. 16. More details about the experimental facility can be seen in [30]. Because the ZrO_2 sphere enters the water at a bigger velocity and decelerates below the

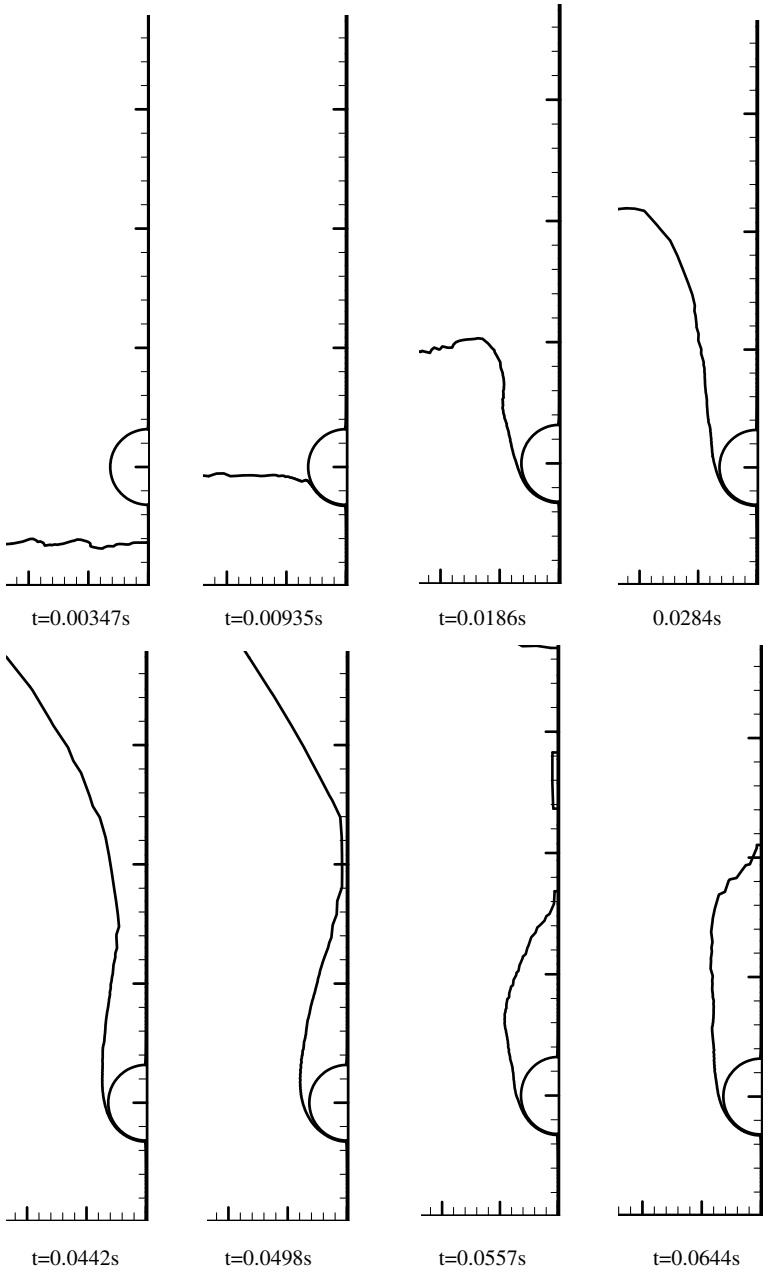

Fig. 14. Movement of liquid–vapor interface in simulation of case 1.

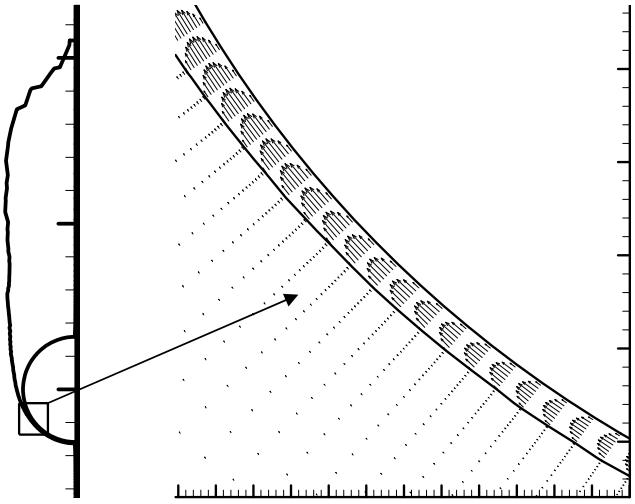

Fig. 15. Velocity field in the vapor film at the front part of the sphere at $t = 0.0644$ s.

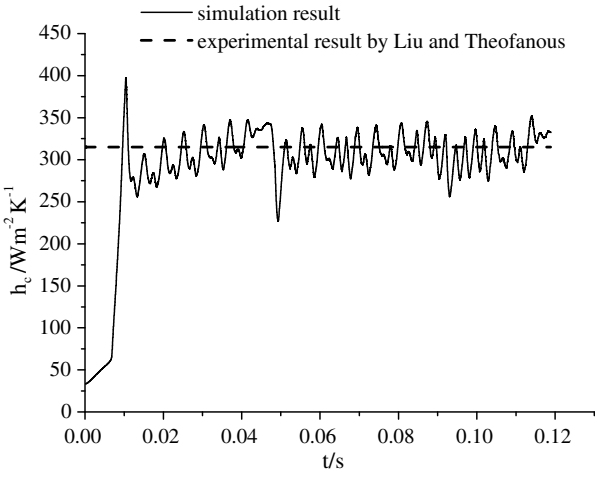

Fig. 17. Convective heat transfer coefficient h_c of case 1.

water surface, the vapor wake is longer than that in simulation. However, the basic feature of the vapor slug detachment from the wake agrees with the experiment observations.

Fig. 17 shows the convective heat transfer coefficient h_c of case 1. The experimental results are displayed for comparison. h_c oscillates in the simulation because of the wavy liquid–vapor interface. As the vapor slug detaches from the vapor wake around $t = 0.05$ s, the oscillation enlarges.

The convective heat transfer coefficients h_c of case 2 and 3 are shown in Figs. 18 and 19. In case 2, the inlet velocity is lower, so the vapor slug detachment point is closer to the sphere. The periodical oscillation due to vapor slug detachment is more obvious. In case 3, the inlet velocity is larger, the high frequency of the liquid–vapor interface fluctuation leads to oscillation of h_c accordingly. In case 3, the vapor wake behind the sphere is very long, so vapor slug detachment does not have obvious influence on h_c.

Figs. 17–19 show that the calculated heat transfer coefficients in these three cases are in a good agreement with the experimental data considering the uncertainty in experiments. It should be noted that radiation from the sphere enhances the production of vapor that goes into the vapor

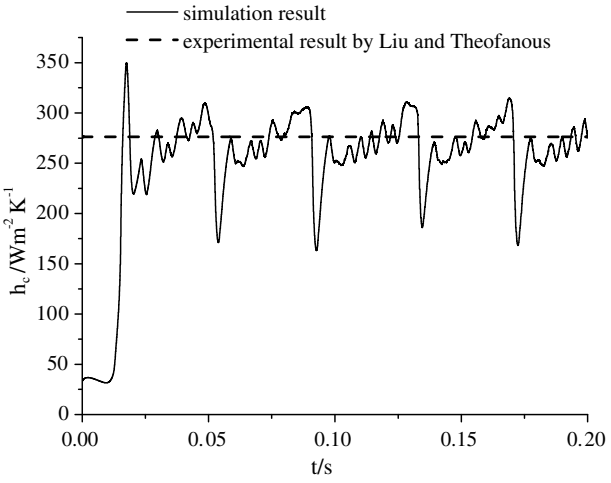

Fig. 18. Convective heat transfer coefficient h_c of case 2.

film, and affects the convective contribution of film boiling. For sphere temperature considered in the experiment, thermal radiation only accounts for about 10–15% of the total heat flux as shown in Table 1. So the influence of radiation on convective heat transfer is not obvious and is not studied here, although radiation has been included in the simulations. In the course of a severe reactor accident, a molten

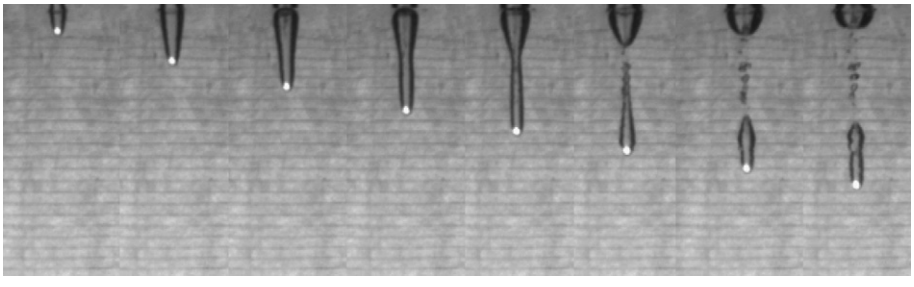

Fig. 16. An experimental picture of a ZrO_2 sphere of diameter 6.35 mm at 1200 K falling to saturate water.

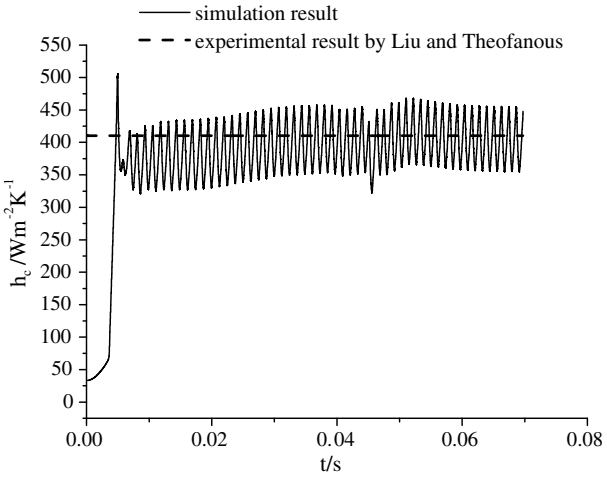

Fig. 19. Convective heat transfer coefficient h_c of case 3.

drop of very high temperature falls through water. In this situation, thermal radiation will become dominant and a further study is needed to investigate the effect of radiant heat.

5. Conclusion

A numerical method for the simulation of boiling flows with non-orthogonal body-fitted coordinates is presented. The volume-of-fluid (VOF) method based on piecewise linear interface construction (PLIC) is extended to body-fitted coordinates, and it is proved to perform as successfully as in Cartesian coordinates. In order to overcome the problem in getting a true volume flux in a discontinuous velocity field due to mass transfer at the liquid–vapor interface, volume expansion or contraction due to mass exchange is moved from a mixture cell where phase change really occurs to the nearest vapor cell. This special treatment is easy to adopt and is proved to be effective in the simulation practice. A double staggered grid with the SIMPLE method is used to solve the flow field.

The method is used to simulate natural convection film boiling and forced convection film boiling on a sphere at saturated conditions. The liquid–vapor interface movement in simulation is in agreement with experimental observations. The parabolic velocity distribution in the thin vapor film which is difficult to observe in experiment is obtained by the numerical simulation. The convective heat transfer coefficients are also consistent with both correlations and experimental data. Obviously, numerical simulations with the interface tracking method to study the transient and dynamic aspects of liquid–vapor phase change have a promising prospect.

Acknowledgement

This work was supported by the National Natural Science Foundation of China (No. 50376036).

References

[1] T.G. Theofanous, W.W. Yuen, The prediction of dynamic loads from ex-vessel steam explosions, in: Proceedings of the International Conference on New Trends in Nuclear System Thermohydraulics, Pisa, 1994, pp. 257–270.
[2] L.C. Witte, Film boiling from a sphere, I and EC Fundam. 7 (3) (1968) 517–518.
[3] T.R. Fodemski, Forced convection film boiling in the stagnation region of molten drop and its application to vapour explosions, Int. J. Heat Mass Transfer 35 (1992) 2005–2016.
[4] T.R. Fodemski, The influence of liquid viscosity and system pressure on stagnation point vapour thickness during forced convection film boiling, Int. J. Heat Mass Transfer 28 (1985) 69–80.
[5] M. Epstein, G.M. Heuser, Subcooled forced-convection film boiling in the forward stagnation region of a sphere or cylinder, Int. J. Heat Mass Transfer 23 (1980) 179–189.
[6] V.K. Dhir, G.P. Purohit, Subcooled film-boiling heat transfer from spheres, Nucl. Eng. Des. 47 (1978) 49–66.
[7] J.W. Stevens, L.C. Witte, Destabilization of vapor film boiling around spheres, Int. J. Heat Mass Transfer 16 (1973) 669–679.
[8] F.J. Walford, Transient heat transfer from a hot Nickel sphere moving through water, Int. J. Heat Mass Transfer 12 (1969) 1621–1625.
[9] C. Liu, T.G. Theofanous, Film boiling on spheres in single- and two-phase Flows. Part 1: Experimental Studies ANS Proceedings, Part 2: A Theoretical Study, National Heat Transfer Conference, Portland, August 1995.
[10] N.I. Kolev, Film boiling on vertical plates and spheres, Exp. Thermal Fluid Sci. 18 (1998) 97–115.
[11] S.W.J. Welch, Local simulation of two-phase flows including interface tracking with mass transfer, J. Comput. Phys. 121 (1995) 142–154.
[12] G. Son, V.K. Dhir, Numerical simulation of saturated film boiling on a horizontal surface, ASME J. Heat Transfer 119 (1997) 525–533.
[13] D. Juric, G. Tryggvason, Computations of boiling flows, Int. J. Multiphase flow 24 (1998) 387–410.
[14] G. Son, V.K. Dhir, Numerical simulation of film boiling near critical pressures with a level set method, ASME J. Heat Transfer 120 (1998) 183–192.
[15] S.W.J. Welch, J.J. Wilson, A volume of fluid based method for fluid flows with phase change, J. Comput. Phys. 160 (2000) 662–682.
[16] C.W. Hirt, B.D. Nichols, Volume of fluid (VOF) method for the dynamics of free boundaries, J. Comput. Phys. 39 (1981) 201–225.
[17] B. Lafaurie, C. Nardone, R. Scardovelli, S. Zaleski, G. Zanetti, Modelling merging and fragmentation in multiphase flows with SURFER, J. Comput. Phys. 113 (1994) 134–147.
[18] N. Ashgriz, J.Y. Poo, FLAIR: flux line-segment model for advection and interface reconstruction, J. Comput. Phys. 93 (1991) 449–468.
[19] D.L. Youngs, Time-dependent multi-material flow with large fluid distortion, in: K.W. Morton, M.J. Baines (Eds.), Numerical Methods for Fluid Dynamics, Academic, New York, 1982, pp. 273–285.
[20] S.V. Patankar, Numerical Heat Transfer and Fluid Flow, McGraw-Hill, New York, 1980.
[21] J.U. Brackbill, D.B. Kothe, C. Zemach, A continuum method for modeling surface tension, J Comput. Phys. 100 (1992) 335–354.
[22] J.H. Ferziger, M. Peric, Computational Methods for Fluid Dynamics, third ed., Springer-Verlag, Berlin, 2001, pp. 225–226.
[23] C.M. Rhie, W.L. Chow, A numerical study of the turbulent flow past an isolated airfoil with trailing edge separation, AIAA J. 21 (1983) 1525–1552.
[24] T.F. Miller, F.W. Schmidt, Use of a pressure-weighted interpolation method for the solution of incompressible Navier–Stokes equations on a non-staggered grid system, Numer. Heat Transfer 14 (1988) 213–233.

[25] A. Shklyar, A. Arbel, Numerical method for calculation of the incompressible flow in general curvilinear co-ordinates with double staggered grid, Int. J. Numer. Meth. Fluids 41 (2003) 1273–1294.
[26] M. Rudman, Volume-tracking methods for interfacial flow calculations, Int. J. Numer. Meth. Fluids 24 (1997) 671–691.
[27] T.H.K. Frederking, J.A. Clark, Natural convection film boiling on a sphere, Adv. Cyrog. Eng. 8 (1962) 501–506.
[28] J.H. Lienhard, A Heat Transfer Textbook, Prentice-Hall Inc., New Jersey, 1981, pp. 411.
[29] R.N. Jacobson, F.M. Shair, Film boiling from a sphere during forced convection of subcooled water, I and EC Fundam. 9 (1970) 183–185.
[30] X.Y. Li, B. Kuang, Y.H. Yang, J.J. Xu, An experimental study on the drag property of high temperature particles falling into cold liquid pool, J. Shanghai Jiaotong University E-8 (1) (2003) 58–62.